Exclusive production of T_{cc}^- in hadron-hadron ultraperipheral collisions

Xiaopeng Wang,[1,2,3] Yaping Xie,[1,3] Yin Huang,[4,*] and Xurong Chen[1,3,†]

[1]Institute of Modern Physics, Chinese Academy of Sciences, Lanzhou 730000, China
[2]School of Nuclear Science and Technology, Lanzhou University, Lanzhou 730000, China
[3]School of Nuclear Science and Technology, University of Chinese Academy of Sciences, Beijing 100049, China
[4]School of Physical Science and Technology, Southwest Jiaotong University, Chengdu 610031, China

(Received 9 October 2023; accepted 13 December 2023; published 8 January 2024)

Understanding the production mechanisms and utilizing them as probes to investigate the structure of exotic states represent some of the most actively studied research areas in particle physics. In this study, we present a theoretical analysis of the charmed meson T_{cc}^- in the $\gamma p \to D^+ T_{cc}^- \Lambda_c^+$ and $\gamma\gamma \to D^+ T_{cc}^- D^{*0}$ reactions, considering T_{cc}^+ as a DD^* molecule. The differential cross section and total cross section for the photoproduction of T_{cc}^- in the $\gamma p \to D^+ T_{cc}^- \Lambda_c^+$ and $\gamma\gamma \to D^+ T_{cc}^- D^{*0}$ reactions are presented for nucleus-nucleus (nucleon-nucleon) ultraperipheral collisions at HL-LHC and RHIC, respectively. Taking into account the integrated luminosity per typical run and the luminosity of photons from the nucleus (nucleon), we observe a significant event count for T_{cc}^- production in p-p ultraperipheral collisions at HL-LHC.

DOI: 10.1103/PhysRevD.109.016007

I. INTRODUCTION

The quark model provides a convenient framework for classifying hadrons, effectively encompassing the majority of hadronic states. Nonetheless, recent significant experimental advancements have led to the observation of numerous exotic hadrons [1,2]. These exotic hadrons exhibit a more complex internal structure than the simple $q\bar{q}$ configuration for mesons or the qqq configuration for baryons in traditional constituent quark models.

The study of exotic hadrons has a long and storied history. However, it entered a new and exciting era in 2003 when the Belle Collaboration made a groundbreaking discovery of the $X(3872)$ in the $\pi^+\pi^- J/\psi$ mass spectra [3]. Based on its observed decay mode, the $X(3872)$ is known to consist of at least four distinct valence quarks, making it a candidate for an exotic hadron. Another well-known exotic hadron candidate is the charged-particle $Z_c^+(3900)$, initially observed by the BESIII Collaboration in the $\pi^\pm J/\psi$ mass spectrum [4]. This observation was later confirmed by the Belle Collaboration in the process $e^+e^- \to \pi^+\pi^- J/\psi$ [5]. Moreover, the LHCb Collaboration has made significant strides in the field by reporting several hidden-charm pentaquark states [6,7].

These discoveries have attracted significant attention to exotic hadron states, particularly those containing charm quarks. Notably, they bring to mind the double-charm meson T_{cc}^+, observed by the LHCb Collaboration in the $D^0D^0\pi^+$ invariant mass spectrum [8]. The mass, width, and quantum numbers of the T_{cc}^+ meson were precisely measured as follows:

$$M = 3875.09\ \text{MeV} + \delta m,$$
$$\Gamma = 48 \pm 2^{+0}_{-14}\ \text{KeV}, \qquad I(J^P) = 0(1^+). \tag{1}$$

Since the mass of T_{cc}^+ lies just below the nominal $D^{*+}D^0$ threshold, it can be interpreted as a hadronic molecule [9–16]. Meanwhile, the compact multiquark structures for T_{cc}^+ are also proposed in Refs. [17,18].

Theoretical investigations on production mechanisms and further experimental information on the production cross section will be helpful to distinguish which inner structure of the T_{cc}^+ state is possible. This dependence arises primarily from the fact that the different yields are strongly influenced by the internal structure of the hadrons. Presently, the photoproduction of T_{cc}^-, which serves as the antiparticle to T_{cc}^+, has undergone investigation as documented in Ref. [19]. The process $\gamma p \to D^+ T_{cc}^- \Lambda_c^+$ involves the utilization of the central diffractive mechanism. In their consideration, the reaction channel involves the exchange of $D^{(*)}$ mesons in the t-channel, while the s- and u-channels are significantly suppressed due to the

*Corresponding author: huangy2019@swjtu.edu.cn
†Corresponding author: xchen@impcas.ac.cn

involvement of two additional $c\bar{c}$ pair creations. Their findings reveal that the total cross section for $\gamma p \to D^+ T_{cc}^- \Lambda_c^+$ is approximately 1 Pb.

When compared to the lower production cross section of the $\gamma p \to D^+ T_{cc}^- \Lambda_c^+$ reaction shown in Ref. [19], ultraperipheral collisions (UPCs) can significantly increase the probability of T_{cc}^- production [20–24]. In UPCs, electromagnetic interactions dominate, occurring when the impact parameter of two ions exceeds the sum of their radii. By employing the Weizsäcker-Williams method [21,24,25], the electromagnetic field originating from highly charged nuclei can be treated as an equivalent flux of photons. As the photon flux is directly proportional to the charge number of ions, highly charged ions offer a substantial photon number density. This suggests that if the $\gamma p \to D^+ T_{cc}^- \Lambda_c^+$ reaction occurs in ultraperipheral collisions, there will be a significant increase in the probability of T_{cc}^- production. Moreover, we also proposed to observe two-photon scattering [24] ($\gamma\gamma \to D^+ T_{cc}^- D^*$) as another part of the search for the T_{cc}^- in UPCs due to the fact that $Z(3930)$, $X(3915)$, and $X(4350)$ were observed in this process by Belle Collaboration [26–28]. As a result, UPCs serve as a crucial platform for investigating the photoproduction of the T_{cc}^- [29,30].

This paper is organized as follows. Theoretical frameworks for the production of T_{cc}^- in $\gamma p \to D^+ T_{cc}^- \Lambda_c^+$ and $\gamma\gamma \to D^+ T_{cc}^- D^*$ in UPCs are presented in Sec. II, respectively. The numerical calculations are given in Sec. III. Finally, a conclusion is given in Sec. IV.

II. THEORETICAL FRAMEWORK

In this work, we investigate the production of T_{cc}^- through one-photon and two-photon processes of UPCs. The corresponding Feynman diagrams are depicted in Figs. 1 and 2. We can find that the high-luminosity photon flux is first emitted from the nucleus or nucleon, resulting in the creation of a pair of high-energy $\bar{D}^* \bar{D}$ mesons. Due to the attractive interaction between $\bar{D}^*$ and $\bar{D}$, a T_{cc}^- molecule is formed in the final state. Next, we will discuss in detail the production mechanisms of T_{cc}^-, corresponding to Figs. 1 and 2, respectively.

A. The production of T_{cc}^- in one-photon process

Within the framework of UPCs, the production cross section of the $A(p)p \to D^+ T_{cc}^- \Lambda_c^+ A(p)$ reaction was given by [31,32]

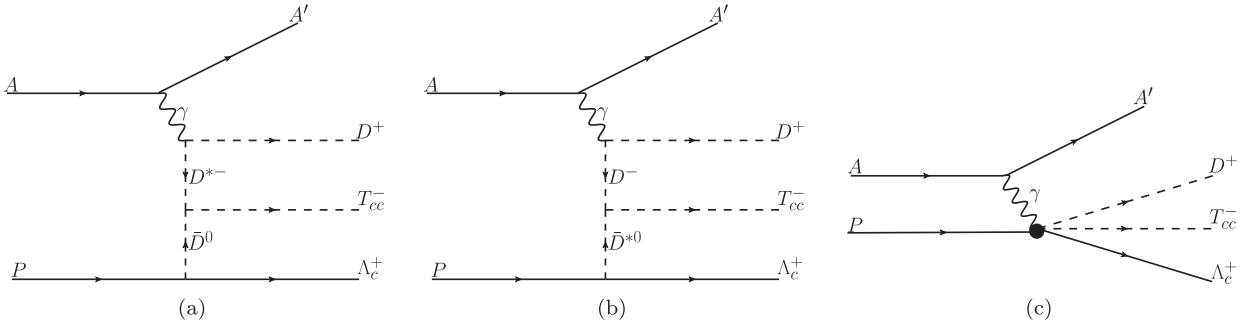

FIG. 1. Production of $p + A \to A + D^+ + T_{cc}^- + \Lambda_c^+$ and $p + p \to p + D^+ + T_{cc}^- + \Lambda_c^+$ in pA or pp UPCs.

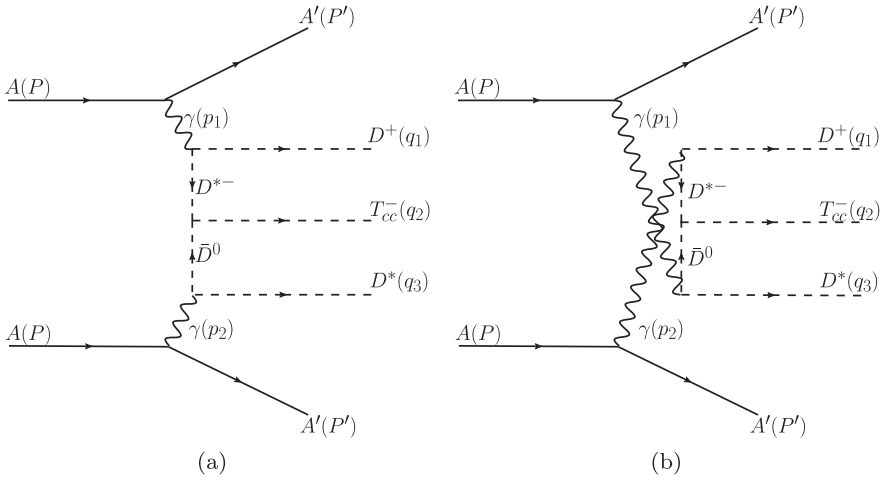

FIG. 2. Two-photon production process for T_{cc}^- in AA, pA, or pp UPCs.

$$\sigma(Ap\to AD^+T_{cc}^-\Lambda_c^+)=\int \mathrm{d}k\frac{\mathrm{d}N_\gamma(k)}{\mathrm{d}k}\sigma_{\gamma p\to D^+T_{cc}^-\Lambda_c^+}(\mathrm{W}), \quad (2)$$

where $\frac{\mathrm{d}N_\gamma(k)}{\mathrm{d}k}$ is the photon flux, with the k representing the energy of the photon emitted from the nucleus (nucleon). W is the center of mass energy of the photon and proton system. Note that $\mathrm{W}=\sqrt{2k\sqrt{s}}$ can be determined based on k and the total energy s of the system. Simplifying, we obtain the W-dependent differential cross section

$$\frac{\mathrm{d}\sigma}{\mathrm{dW}}=\left(\frac{\mathrm{d}N_\gamma(k)}{\mathrm{d}k}\frac{\mathrm{W}}{\sqrt{s}}\right)\sigma_{\gamma p\to D^+T_{cc}^-\Lambda_c^+}(\mathrm{W}). \quad (3)$$

In order to make a reliable prediction for the cross section of the $A(p)p\to D^+T_{cc}^-\Lambda_c^+A(p)$ reaction, we need to address the following two key issues: the value of the photon flux and the $\sigma_{\gamma p\to D^+T_{cc}^-\Lambda_c^+}(\mathrm{W})$. The photon flux from the nucleus is described by the equation [33]

$$\frac{\mathrm{d}N_\gamma(k)}{\mathrm{d}k}=\frac{2Z^2\alpha_{em}}{\pi k}\left(\xi K_0(\xi)K_1(\xi)-\frac{\xi^2}{2}[K_1^2(\xi)-K_0^2(\xi)]\right), \quad (4)$$

where K_0 and K_1 are modified Bessel functions, Z is the ion charge, $\alpha_{em}=1/137$, and $\xi=b_{\min}k/\gamma_{\mathrm{L}}$ with $\gamma_{\mathrm{L}}=\sqrt{s}/(2m_p)$ represents the Lorentz boost factor. The value of $b_{\min}=R_A+R_p$ is the sum of the nucleus and proton charge radius, where R_A is often defined as [34]

$$R_A=(1.12A^{1/3}-0.86A^{-1/3})\ (\mathrm{fm}). \quad (5)$$

It is important to note that the photon flux emitted from the proton differs from the photon flux from the nucleus, and it can be expressed using the dipole form factor [21,35]

$$\frac{dn}{dk}(k)=\frac{\alpha_{em}}{2\pi k}\left[1+\left(1-\frac{2k}{\sqrt{s}}\right)^2\right]\times\left(\ln\Omega-\frac{11}{6}+\frac{3}{\Omega}-\frac{3}{2\Omega^2}+\frac{1}{3\Omega^3}\right), \quad (6)$$

where $\Omega=1+0.71\ \mathrm{GeV}^2/Q_{\min}^2$ and $Q_{\min}^2=k^2/\gamma_{\mathrm{L}}^2$ represents the minimum momentum transfer possible in the reaction.

The differential cross section in the c.m. frame for the $\gamma p\to D^+T_{cc}^-\Lambda_c^+$ reaction reads

$$d\sigma(\gamma p\to D^+T_{cc}^-\Lambda_c^+)=\frac{1}{(2\pi)^5}\frac{1}{4(k_1\cdot k_2)}\bar{\sum_{s_i,s_f}}|-i\mathcal{M}(\gamma p\to D^+T_{cc}^-\Lambda_c^+)|^2\times\frac{d^3\vec{p}_1}{2E_1}\frac{d^3\vec{p}_2}{2E_2}\frac{d^3\vec{p}_3}{2E_3}\delta^4(k_1+k_2-p_1-p_2-p_3), \quad (7)$$

where E_1, E_2, E_3 and p_1, p_2, p_3 stand for the energies and four-momentum of D^+, $\bar{T}_{cc}^-$, and Λ_c^+, respectively. k_1 and k_2 are the four-momentum of the initial photon and proton, respectively, and m_p and $m_{\Lambda_c^+}$ are the masses of the proton and Λ_c^+, respectively. The $\mathcal{M}(\gamma p\to D^+T_{cc}^-\Lambda_c^+)$ represents the total scattering amplitude for the $\gamma p\to D^+T_{cc}^-\Lambda_c^+$ reaction, which has been computed in Ref. [19],

$$-i\mathcal{M}=\bar{u}(p_3,\lambda_{\Lambda_c^+})\sum_{j=a,b,c}\mathcal{W}_j^{\mu\nu}u(k_2,\lambda_p)\times\epsilon_\nu(k_1,\lambda_\gamma)\epsilon_\mu^*(p_2,\lambda_{\bar{T}_{cc}^-}), \quad (8)$$

with

$$\mathcal{W}_a^{\mu\nu}=-g_{D^*D\gamma}g_{DN\Lambda_c}g_{\bar{T}_{cc}}\gamma_5\epsilon_{\alpha\nu\beta\rho}k_1^\alpha q_1^\beta\times\frac{-g^{\mu\rho}+q_1^\mu q_1^\rho/m_{D^{*-}}^2}{q_1^2-m_{D^{*-}}^2}\frac{\mathcal{F}_{\bar{D}^0}\mathcal{F}_{D^{*-}}}{q_2^2-m_{\bar{D}^0}^2}, \quad (9)$$

$$\mathcal{W}_b^{\mu\nu}=-ieg_{D^*N\Lambda_c}g_{\bar{T}_{cc}}\gamma_\rho(q_1^\nu-p_1^\nu)\times\frac{-g^{\mu\rho}+q_2^\mu q_2^\rho/m_{\bar{D}^{*0}}^2}{q_2^2-m_{\bar{D}^{*0}}^2}\frac{\mathcal{F}_{\bar{D}^{*0}}\mathcal{F}_{D^-}}{q_1^2-m_{D^-}^2}, \quad (10)$$

$$\mathcal{W}_c^{\mu\nu}=-i2eg_{D^*N\Lambda_c}g_{\bar{T}_{cc}}\left(-\gamma_\mu+\frac{m_p-m_{\Lambda_c^+}}{m_{\bar{D}^{*0}}^2}q_{2\mu}\right)\times\frac{k_1^\nu-p_1^\nu}{q_2^2-m_{\bar{D}^{*0}}^2}\frac{\mathcal{F}_{\bar{D}^{*0}}\mathcal{F}_{D^-}}{q_1^2-m_{D^-}^2}, \quad (11)$$

where they correspond to the Feynman diagrams as well as the contact terms discussed in Ref. [19], respectively. In the above equation, u and ϵ are the Dirac spinor and polarization vector, respectively, and λ is the helicity. Coupling constants $g_{DN\Lambda_c}=-13.98$ and $g_{D^*N\Lambda_c}=-5.20$ are computed from the SU(4) invariant Lagrangians in terms of $g_{\pi NN}=13.45$ and $g_\rho NN=6$ [36–38]. $g_{D^*D\gamma}=0.173$–$0.228\ \mathrm{GeV}^{-1}$ is determined by the radiative decay widths of D^* [39]. The coupling constants $g_{T_{cc}D^{*+}D^0}=3.67$ GeV and $g_{T_{cc}D^0D^+}=-3.92$ GeV are derived from chiral unitary theory, where T_{cc} is identified as an S-wave D^*D molecule [40]. $e=\sqrt{4\pi\alpha}$ with α being the fine-structure constant, and $\epsilon^{\mu\nu\alpha\beta}$ is the Levi-Civita tensor.

Considering the internal structure of the exchange mesons, the form factor must be taken into account. In this work, the monopole form factors $\mathcal{F}_{\bar{D}^{(*)0}}$ and $\mathcal{F}_{D^{(*)-}}$ that can be found in Eqs. (9)–(11) are utilized, as shown in [19],

$$\mathcal{F}_i=\frac{\Lambda_i^2-m_i^2}{\Lambda_i^2-t_i},\qquad i=\bar{D}^0,D^{*-}, \quad (12)$$

where m_i and t_i represent the mass and the four-momentum square of exchange mesons $\bar{D}^0$ or D^{*-}. The cutoff $\Lambda_i=m_i+\alpha\Lambda_{\mathrm{QCD}}$, where α is a parameter related to the

nonperturbative property of QCD at the low-energy scale. In Ref. [19], $\Lambda_{\rm QCD} = 0.22,$ GeV is adopted, and $\alpha = 1.5$ or 1.7 is computed by fitting the experimental data [41–43].

B. The production of T_{cc}^- in the two-photon process

The Feynman diagram for the production of T_{cc}^- in the two-photon process of UPCs is plotted in Fig. 2. The relevant differential cross section is expressed as

$$\frac{d\sigma_{AB}}{d\mathrm{W}_{\gamma\gamma}} = \frac{d\mathcal{L}_{\gamma\gamma}^{AB}}{d\mathrm{W}_{\gamma\gamma}} \sigma_{\gamma\gamma\to D^+ T_{cc}^- D^*}(\mathrm{W}_{\gamma\gamma}), \tag{13}$$

where A and B represent the nucleus or proton, $\sigma_{\gamma\gamma\to D^+ T_{cc}^- D^*}$ denotes the total cross section of the two-photon T_{cc}^- production process, and $\mathrm{W}_{\gamma\gamma}$ stands for the center-of-mass energy of the two-photon system. The effective two-photon luminosity, denoted as $\frac{d\mathcal{L}_{\gamma\gamma}^{AB}}{d\mathrm{W}_{\gamma\gamma}}$, can be obtained from the gamma-UPC package [44]. The effective two-photon luminosity is defined as

$$\frac{\mathrm{d}\mathcal{L}_{\gamma\gamma}^{(\mathrm{AB})}}{\mathrm{d}W_{\gamma\gamma}} = \frac{2W_{\gamma\gamma}}{s}\int \frac{\mathrm{d}E_{\gamma_1}}{E_{\gamma_1}}\frac{\mathrm{d}E_{\gamma_2}}{E_{\gamma_2}} \times \delta\left(\frac{W_{\gamma\gamma}^2}{s} - \frac{4E_{\gamma_1}E_{\gamma_2}}{s}\right)\frac{\mathrm{d}^2 N_{\gamma_1/\mathrm{Z}_1,\gamma_2/\mathrm{Z}_2}^{(\mathrm{AB})}}{\mathrm{d}E_{\gamma_1}\mathrm{d}E_{\gamma_2}}, \tag{14}$$

where $\mathrm{W}_{\gamma\gamma}$ is the center-of-mass energy of two-photon, s is the square of center-of-mass energy of proton-proton, proton-nucleus, or nucleus-nucleus. The two-photon differential yield, $\frac{\mathrm{d}^2 N_{\gamma_1/\mathrm{Z}_1,\gamma_2/\mathrm{Z}_2}^{(\mathrm{AB})}}{\mathrm{d}E_{\gamma_1}\mathrm{d}E_{\gamma_2}}$, is written as

$$\frac{\mathrm{d}^2 N_{\gamma_1/\mathrm{Z}_1,\gamma_2/\mathrm{Z}_2}^{(\mathrm{AB})}}{\mathrm{d}E_{\gamma_1}\mathrm{d}E_{\gamma_2}} = \int \mathrm{d}^2\boldsymbol{b}_1\mathrm{d}^2\boldsymbol{b}_2 P_{\text{no inel}}(|\boldsymbol{b}_1-\boldsymbol{b}_2|) \times N_{\gamma_1/\mathrm{Z}_1}(E_{\gamma_1},\boldsymbol{b}_1)N_{\gamma_2/\mathrm{Z}_2}(E_{\gamma_2},\boldsymbol{b}_2) \times \theta(b_1-\epsilon R_{\mathrm{A}})\theta(b_2-\epsilon R_{\mathrm{B}}), \tag{15}$$

where $P_{\text{no inel}}(|\boldsymbol{b}_1-\boldsymbol{b}_2|)$ represents the probability of the absence of an inelastic hadronic interaction at the impact parameter $|\boldsymbol{b}_1-\boldsymbol{b}_2|$. The photon flux, denoted as $N_{\gamma/\mathrm{Z}}(E_\gamma,\boldsymbol{b})$, employed in our study is determined by the electric dipole form factor (EDFF) of the emitting nucleus or proton. So, its precise form can be expressed as follows:

$$N_{\gamma/\mathrm{Z}}^{\mathrm{EDFF}}(E_\gamma,b) = \frac{Z^2\alpha}{\pi^2}\frac{\xi^2}{b^2}\left[K_1^2(\xi)+\frac{1}{\gamma_{\mathrm{L}}^2}K_0^2(\xi)\right]. \tag{16}$$

Here, Z represents the charge number, and $\xi = bE_\gamma/\gamma_{\mathrm{L}}$, where γ_{L} is the Lorentz boost factor. K_1 and K_0 are modified Bessel functions. In the special case when $\mathrm{Z}=1$ and $P_{\text{no inel}}=1$, the photon distribution function is obtained by integrating Eq. (16) over b as follows:

$$n_{\gamma/p}^{\mathrm{EDFF}}(x) = n_{\gamma/p}(xR_p m_p), \tag{17}$$

where $x = E_\gamma/E_p$, and $n_{\gamma/p}(\chi)$ is denoted by

$$n_{\gamma/p}(\chi) = \frac{2\alpha}{\pi}\left[\chi K_0(\chi)K_1(\chi) - (1-\gamma_{\mathrm{L}}^{-2})\frac{\chi^2}{2}(K_1^2(\chi)-K_0^2(\chi))\right]. \tag{18}$$

Note that we provide a brief introduction to the effective two-photon luminosity used in our study. More details can be found in Ref. [44]. In addition, the two-photon T_{cc}^- production cross section is unknown and will be discussed later.

To compute the two-photon T_{cc}^- production cross section $\sigma_{\gamma\gamma\to D^+T_{cc}^-D^*}$, the effective Lagrangians with the smallest number of derivatives are given as follows [1,19,45–47]:

$$\mathcal{L}_{T_{cc}D^*D} = g_{T_{cc}D^*D}T_{cc}^{\mu\dagger}D_\mu^* D,$$
$$\mathcal{L}_{\gamma DD^*} = g_{\gamma DD^*}\epsilon_{\mu\nu\alpha\beta}(\partial^\mu\mathcal{A}^\nu)(\partial^\alpha D^{*\beta})D + \mathrm{H.c.}, \tag{19}$$

where T_{cc}^μ, D_μ^*, D, and $\mathcal{A}^\mu$ represent the T_{cc}^- meson, the D^* meson, the D meson, and the photon, respectively.

Then, as shown in Figs. 2(a) and 2(b) for the two-photon T_{cc}^- production, the invariant amplitude of $\gamma\gamma\to D^+T_{cc}^-D^*$ is written as

$$-i\mathcal{M} = \epsilon_\theta^*(q_3)\epsilon_\mu^*(q_2)(\mathcal{W}_{(a)}^{\theta\mu\nu\alpha}+\mathcal{W}_{(b)}^{\theta\mu\nu\alpha})\epsilon_\nu(p1)\epsilon_\alpha(p2). \tag{20}$$

In the amplitude, $\mathcal{W}_{(a)}^{\theta\mu\nu\alpha}$ and $\mathcal{W}_{(b)}^{\theta\mu\nu\alpha}$ are similar. They are constructed as

$$\mathcal{W}_{(a)}^{\theta\mu\nu\alpha} = g_a\mathcal{F}_a\epsilon_{\beta\nu\eta\rho}p_1^\beta k_1^\eta\frac{-g^{\mu\rho}+k_1^\mu k_1^\rho/m_{D^{*-}}^2}{k_1^2-m_{D^{*-}}^2} \times\frac{1}{k_2^2-m_{\bar{D}^0}^2}\epsilon_{e\alpha f\theta}p_2^e q_3^f, \tag{21}$$

$$\mathcal{W}_{(b)}^{\theta\mu\nu\alpha} = g_a\mathcal{F}'_a\epsilon_{\beta\nu\eta\rho}p_2^\beta k'^\eta_1\frac{-g^{\mu\rho}+k'^\mu_1 k'^\rho_1/m_{D^{*-}}^2}{k'^2_1-m_{D^{*-}}^2} \times\frac{1}{k'^2_2-m_{\bar{D}^0}^2}\epsilon_{e\alpha f\theta}p_1^e q_3^f, \tag{22}$$

where $g_a = g_{T_{cc}D^{*-}\bar{D}^0}g_{\gamma D^+D^{*-}}g_{\gamma\bar{D}^0D^{*0}}$ and $\mathcal{F}_a = \mathcal{F}_{D^{*-}}\mathcal{F}_{\bar{D}^0}$.

The differential cross section for two-photon T_{cc}^- production can be described as follows:

$$d\sigma_{\gamma\gamma} = \frac{1}{(2\pi)^5}\frac{1}{4\sqrt{(p_1\cdot p_2)^2}}|\bar{\mathcal{M}}|^2 \times\delta^4(p_1+p_2-q_1-q_2-q_3)\frac{d^3\vec{q}_1}{2q_1^0}\frac{d^3\vec{q}_2}{2q_2^0}\frac{d^3\vec{q}_3}{2q_3^0}, \tag{23}$$

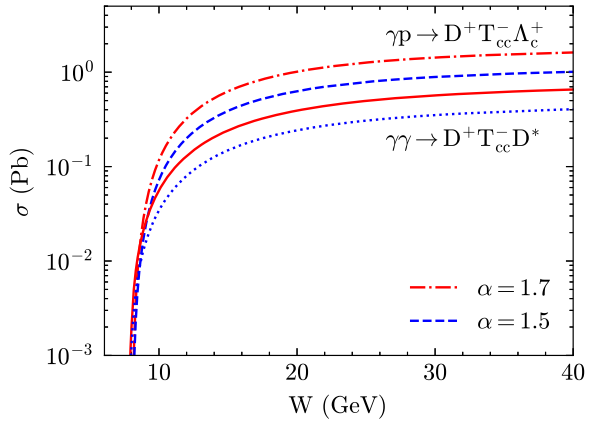

FIG. 3. Total cross sections for the $\gamma p \to D^+ T_{cc}^- \Lambda_c^+$ (dot-dashed line and dashed line) and for the $\gamma\gamma \to D^+ T_{cc}^- D^*$ (solid line and dotted line) as a function of W while $\alpha = 1.7$ (red lines) or $\alpha = 1.5$ (blue lines).

where $\overline{|\mathcal{M}|}$ represents the final-state spin summation and the initial-state spin averaging of the scattering amplitude. Finally, the total cross section, obtained by integrating the differential cross section with the 3BODYXSECTIONS package [48], will be presented as a function of the center-of-mass energy W.

III. NUMERICAL RESULTS

In this study, we estimate the production cross section of T_{cc}^- through one-photon and two-photon processes in UPCs. To achieve these results, we need to initially evaluate the cross sections for the $\gamma\gamma \to D^+ T_{cc}^- D^*$ and $\gamma p \to D^+ T_{cc}^- \Lambda_c^+$ reactions, as indicated in Eqs. (3) and (13). These cross sections can be computed by integrating the differential cross section based on the 3BODYXSECTIONS package [48]. The equations expressing the differential cross section for these two reactions can be found in Eqs. (7) and (23).

The cross sections of the $\gamma p \to D^+ T_{cc}^- \Lambda_c^+$ and the $\gamma\gamma \to D^+ T_{cc}^- D^*$ reactions are depicted against W for $\alpha = 1.5$ and $\alpha = 1.7$ in Fig. 3, respectively. We can find that when the energy approaches the $D^+ T_{cc}^- D^*$ threshold, the total cross section increases sharply. At higher energies, the cross section increases continuously but relatively slowly compared with that near threshold. Our numerical results also show that the total cross section for $\alpha = 1.7$ is larger than that of $\alpha = 1.5$, but the disparity is not significant. To provide an example, let us examine the cross section at an energy of around W = 40 GeV. In this instance, the obtained cross section ranges from 1.0 Pb to 1.62 Pb for $\gamma p \to D^+ T_{cc}^- \Lambda_c^+$ and from 0.405 pb to 0.655 pb for $\gamma\gamma \to D^+ T_{cc}^- D^*$, respectively, when altering the value of α from 1.5 to 1.7. Therefore, in the following calculations, we only provide the results with $\alpha = 1.5$. By comparing the cross sections depicted in Fig. 3, we find that the total cross section for T_{cc}^- production in the $\gamma p \to D^+ T_{cc}^- \Lambda_c^+$ reaction is bigger than that of the T_{cc}^- production in the $\gamma\gamma \to D^+ T_{cc}^- D^*$ reaction.

With the above obtained cross section, we present the differential cross sections for one-photon T_{cc}^- production in UPCs as a function of the W of the photon-nucleus system at $\sqrt{s} = 8.8$ TeV for the p-Pb system and $\sqrt{s} = 200$ GeV for the p-Au system, as illustrated in Fig. 4. We can find that the differential cross sections for the p-Pb system are greater than those of the p-Au system. One possible explanation for this is that the photon flux is directly proportional to the charge number of the nucleus. Moreover, our results suggest that the differential cross sections are notably significant in the low-energy range. As the energy increases, the differential cross sections decrease rapidly.

Next, we calculate the differential cross sections through two-photon T_{cc}^- production in nucleus-nucleus and proton-proton UPCs, as illustrated in Fig. 5. These calculations are performed for collision energies of $\sqrt{s}$= 5.5 TeV for the Pb-Pb system, $\sqrt{s} = 7$ TeV for the oxygen-oxygen (O-O) system, and $\sqrt{s} = 14$ TeV for the p-p system, respectively. Moreover, for the p-Pb system and the p-Au system,

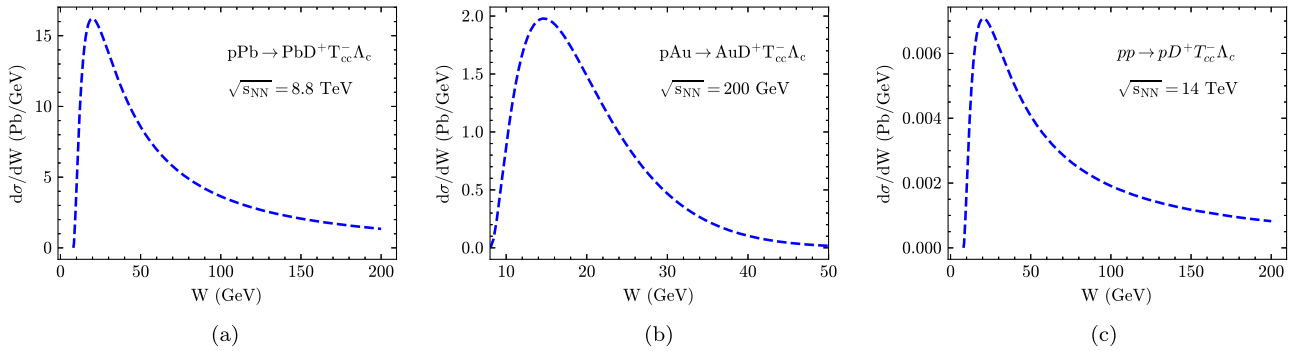

FIG. 4. Differential cross section as a function of W of one-photon T_{cc}^- production while the subprocess is $\gamma p \to D^+ T_{cc}^- \Lambda_c$ in p-Pb, p-Au, p-p UPCs, respectively (from left to right).

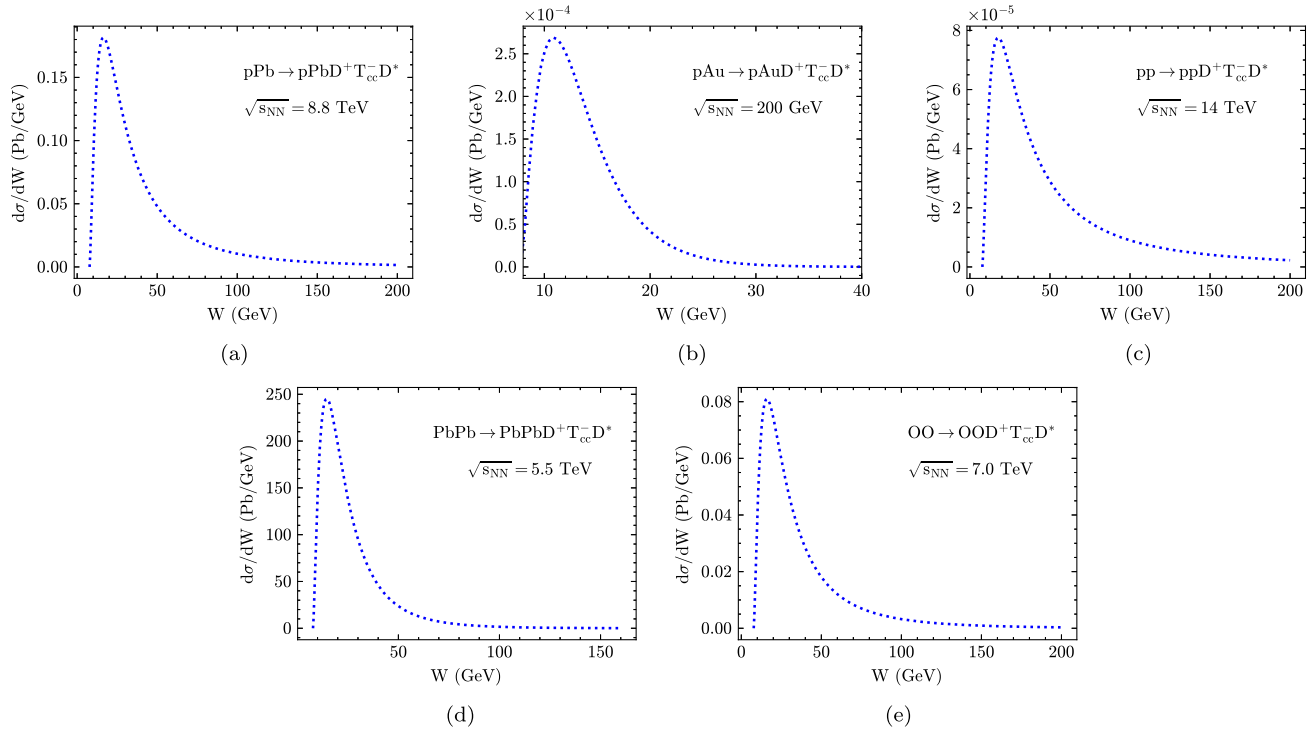

FIG. 5. The differential cross section $d\sigma/dW$ of two-photon T_{cc}^- production while the subprocess is $\gamma\gamma \to D^+T_{cc}^-D^*$ in p-Pb, p-Au, p-p, Pb-Pb, and O-O UPCs, respectively.

we present the differential cross sections against the center-of-mass energy W, depicted in Fig. 5, for collision energies of $\sqrt{s} = 8.8$ TeV and $\sqrt{s} = 200$ GeV, respectively. It can be observed that the primary contribution of the two-photon process takes place within a distinct low center-of-mass energy range, similar to that of one-photon T_{cc}^- production. Notably, T_{cc}^- production in Pb-Pb UPCs is the largest due to the higher luminosity of the photon flux originating from Pb.

Finally, we list the predicted event numbers for one-photon and two-photon T_{cc}^- production in the Pb-Pb system, the O-O system, the Pb-p system, the Au-p system, and the p-p system, respectively, in Table I. We can find that the total cross section $\sigma_{\rm tot}$ for the one-photon $\gamma p \to D^+T_{cc}^-\Lambda_c^+$ process is smaller in the p-p system compared to the Pb-p and Au-p systems. However, due to the higher integrated luminosity per typical run $\mathcal{L}_{\rm int}$ in the p-p system, the event number is larger than that of the other processes. Conversely, it is noticeable that in the case of the two-photon process, the total cross sections are smaller compared to those of the one-photon process in the Pb-p, Au-p, and p-p systems. Despite the total cross section $\sigma_{\rm tot}$ reaching approximately 5 nb for the two-photon T_{cc}^- process in the Pb-Pb system, owing to the very high two-photon number densities, the restricted luminosity results in a relatively small number of events. As a result, identifying T_{cc}^- through the one-photon process is more feasible.

TABLE I. 1. Integrated luminosity per typical run $\mathcal{L}_{\rm int}$ and c.m. energy $\sqrt{s_{NN}}$ of nucleus (proton)–nucleus (proton) UPCs from HL-LHC and RHIC [44,49–51]. 2. The total cross sections and the event numbers of one-photon and two-photon T_{cc}^- production in different kinds of UPCs.

			$\sigma_{\rm tot}$ (pb)		Events	
System	$\sqrt{s_{NN}}$	$\mathcal{L}_{\rm int}$ ($\rm pb^{-1}$)	One-photon	Two-photon	One-photon	Two-photon
Pb-Pb	5.5 TeV	5×10^{-3}	⋯	5191	⋯	25.9
O-O	7.0 TeV	12	⋯	2.5	⋯	30
Pb-p	8.8 TeV	1	1000	6.0	1000	6.0
Au-p	200 GeV	4.5	30.1	0.002	135.5	< 1
p-p	14 TeV	1.5×10^5	0.48	0.0035	7.2×10^4	525

IV. CONCLUSION

In this work, theoretical frameworks of one-photon and two-photon T_{cc}^- production are introduced. Then the differential distribution and the total cross section of one-photon and two-photon T_{cc}^- production in UPCs are calculated. At last, the events of T_{cc}^- production are estimated in different collision systems.

Based on the work of [19] for $\gamma p \to D^+ T_{cc}^- \Lambda_c$, the differential cross sections as a function of the center-of-mass energy of photon and proton (W) in Pb-p, Au-p, and p-p collisions are calculated. And referring to the $\gamma p \to D^+ T_{cc}^- \Lambda_c$ process, the t-channel amplitude of $\gamma\gamma \to D^+ T_{cc}^- D^*$ is presented. Then the differential cross sections for two-photon T_{cc}^- UPCs in different collision systems are shown. At last, the events of one-photon and two-photon T_{cc}^- production are estimated, respectively. Due to high-luminosity photon flux in Pb-p and Pb-Pb systems, the total cross section of the one-photon UPC process for T_{cc}^- production is approximately 1 nb and the total cross section of the two-photon UPC process for T_{cc}^- production is approximately 5 nb, respectively. But because of the limited integrated luminosity in Pb-p and Pb-Pb systems, the number of events is lower. In the p-p system, despite the lower production cross section of T_{cc}^-, the higher number of events is generated due to the integrated luminosity being about $1.5 \times 10^5 \mathrm{Pb}^{-1}$. In conclusion, it is more possible to identify T_{cc}^- in p-p UPCs in the future HL-LHC.

ACKNOWLEDGMENTS

This work is supported by the Strategic Priority Research Program of Chinese Academy of Sciences under Grant No. XDB34030301, the National Natural Science Foundation of China under Grant No. 12005177, and Guangdong Major Project of Basic and Applied Basic Research No. 2020B0301030008.

[1] F.-K. Guo, C. Hanhart, U.-G. Meißner, Q. Wang, Q. Zhao, and B.-S. Zou, Rev. Mod. Phys. **90**, 015004 (2018); **94**, 029901(E) (2022).
[2] H.-X. Chen, W. Chen, X. Liu, Y.-R. Liu, and S.-L. Zhu, Rep. Prog. Phys. **86**, 026201 (2023).
[3] S. K. Choi *et al.* (Belle Collaboration), Phys. Rev. Lett. **91**, 262001 (2003).
[4] M. Ablikim *et al.* (BESIII Collaboration), Phys. Rev. Lett. **110**, 252001 (2013).
[5] Z. Q. Liu *et al.* (Belle Collaboration), Phys. Rev. Lett. **110**, 252002 (2013); **111**, 019901(E) (2013).
[6] R. Aaij *et al.* (LHCb Collaboration), Phys. Rev. Lett. **115**, 072001 (2015).
[7] R. Aaij *et al.* (LHCb Collaboration), Sci. Bull. **66**, 1278 (2021).
[8] R. Aaij *et al.* (LHCb Collaboration), Nat. Commun. **13**, 3351 (2022).
[9] M. Albaladejo, Phys. Lett. B **829**, 137052 (2022).
[10] V. Montesinos, M. Albaladejo, J. Nieves, and L. Tolos, Phys. Rev. C **108**, 035205 (2023).
[11] M.-L. Du, V. Baru, X.-K. Dong, A. Filin, F.-K. Guo, C. Hanhart, A. Nefediev, J. Nieves, and Q. Wang, Phys. Rev. D **105**, 014024 (2022).
[12] S. S. Agaev, K. Azizi, and H. Sundu, Nucl. Phys. **B975**, 115650 (2022).
[13] L. Meng, G.-J. Wang, B. Wang, and S.-L. Zhu, Phys. Rev. D **104**, L051502 (2021).
[14] M.-J. Yan and M. P. Valderrama, Phys. Rev. D **105**, 014007 (2022).
[15] X.-Z. Ling, M.-Z. Liu, L.-S. Geng, E. Wang, and J.-J. Xie, Phys. Lett. B **826**, 136897 (2022).
[16] G.-J. Wang, Z. Yang, J.-J. Wu, M. Oka, and S.-L. Zhu, arXiv:2306.12406.
[17] Y. Kim, M. Oka, and K. Suzuki, Phys. Rev. D **105**, 074021 (2022).
[18] E. J. Eichten and C. Quigg, Phys. Rev. Lett. **119**, 202002 (2017).
[19] Y. Huang, H. Q. Zhu, L.-S. Geng, and R. Wang, Phys. Rev. D **104**, 116008 (2021).
[20] A. Esposito, C. A. Manzari, A. Pilloni, and A. D. Polosa, Phys. Rev. D **104**, 114029 (2021).
[21] C. A. Bertulani, S. R. Klein, and J. Nystrand, Annu. Rev. Nucl. Part. Sci. **55**, 271 (2005).
[22] G. Baur, K. Hencken, D. Trautmann, S. Sadovsky, and Y. Kharlov, Phys. Rep. **364**, 359 (2002).
[23] F. Krauss, M. Greiner, and G. Soff, Prog. Part. Nucl. Phys. **39**, 503 (1997).
[24] A. J. Baltz, Phys. Rep. **458**, 1 (2008).
[25] E. J. Williams, Phys. Rev. **45**, 729 (1934).
[26] S. Uehara *et al.* (Belle Collaboration), Phys. Rev. Lett. **96**, 082003 (2006).
[27] S. Uehara *et al.* (Belle Collaboration), Phys. Rev. Lett. **104**, 092001 (2010).
[28] C. P. Shen *et al.* (Belle Collaboration), Phys. Rev. Lett. **104**, 112004 (2010).
[29] S. R. Klein and Y.-P. Xie, Phys. Rev. C **100**, 024620 (2019).
[30] Y.-P. Xie, X.-Y. Wang, and X. Chen, Eur. Phys. J. C **81**, 710 (2021).
[31] S. R. Klein, J. Nystrand, J. Seger, Y. Gorbunov, and J. Butterworth, Comput. Phys. Commun. **212**, 258 (2017).
[32] Y.-P. Xie, X.-Y. Wang, and X. Chen, Chin. Phys. C **45**, 014107 (2021).
[33] S. R. Klein and J. Nystrand, Phys. Rev. C **60**, 014903 (1999).
[34] T. Lappi and H. Mantysaari, Phys. Rev. C **83**, 065202 (2011).

[35] M. Drees and D. Zeppenfeld, Phys. Rev. D **39**, 2536 (1989).
[36] Y. Dong, A. Faessler, T. Gutsche, S. Kumano, and V. E. Lyubovitskij, Phys. Rev. D **82**, 034035 (2010).
[37] Y. Huang, J. He, J.-J. Xie, and L.-S. Geng, Phys. Rev. D **99**, 014045 (2019).
[38] S. Okubo, Phys. Rev. D **11**, 3261 (1975).
[39] P. A. Zyla *et al.*, Prog. Theor. Exp. Phys. **2020**, 083C01 (2020).
[40] A. Feijoo, W. H. Liang, and E. Oset, Phys. Rev. D **104**, 114015 (2021).
[41] X.-D. Guo, D.-Y. Chen, H.-W. Ke, X. Liu, and X.-Q. Li, Phys. Rev. D **93**, 054009 (2016).
[42] B. Aubert *et al.* (*BABAR* Collaboration), Phys. Rev. D **76**, 111105 (2007).
[43] G. Pakhlova *et al.* (Belle Collaboration), Phys. Rev. D **77**, 011103 (2008).
[44] H.-S. Shao and D. d'Enterria, J. High Energy Phys. 09 (2022) 248.
[45] F.-K. Guo, C. Hanhart, Y. Kalashnikova, U.-G. Meißner, and A. Nefediev, Phys. Lett. B **742**, 394 (2015).
[46] M.-L. Du, V. Baru, F.-K. Guo, C. Hanhart, U.-G. Meißner, A. Nefediev, and I. Strakovsky, Eur. Phys. J. C **80**, 1053 (2020).
[47] Y. Huang, C.-j. Xiao, Q. F. Lü, R. Wang, J. He, and L. Geng, Phys. Rev. D **97**, 094013 (2018).
[48] J. C. Romao, Computational techniques in quantum field theory, http://porthos.ist.utl.pt/CTQFT/.
[49] R. Bruce *et al.*, J. Phys. G **47**, 060501 (2020).
[50] D. d'Enterria *et al.*, J. Phys. G **50**, 050501 (2023).
[51] M. Tanabashi *et al.* (Particle Data Group Collaboration), Phys. Rev. D **98**, 030001 (2018).